Photoproduction of the π^0 meson from 1.1 - 5.5 GeV and a comparison to the CCR and Handbag model

M. C. Kunkel* and M. J. Amaryan
Old Dominion University, VA (U.S.A.)

I. Strakovsky
The George Washington University, Washington, DC (U.S.A.)

(and the CLAS Collaboration)

(Dated: June 9, 2016)

Exclusive neutral pion photoproduction ($\gamma p \rightarrow p\pi^0$) was measured in the CLAS detector at the Thomas Jefferson National Facility. The experiment employed a 1.1-5.5 GeV bremsstrahlung photon beam from 5.6 GeV electron beam created in the Continuous Electron Beam Accelerator Facility (CEBAF). The photon beam energy was impinged on a liquid hydrogen target. The neutral pions were detected via external conversion, $\pi^0 \rightarrow \gamma\gamma \rightarrow e^+e^-\gamma$, and subsequent Dalitz decay, $\pi^0 \rightarrow \gamma^*\gamma \rightarrow e^+e^-\gamma$. Measured differential cross-sections, $\frac{d\sigma}{dt}$ and $\frac{d\sigma}{d\cos\theta}$ are compared with the constituent counting rule, Regge and handbag theoretical calculations. The results for the constituent counting rule agree well with the data. The Regge theoretical calculations underestimate the differential cross sections between 3.9 and 4.6 GeV, but agree with data at photon energies 4.6-5.4 GeV. The handbag theoretical calculation significantly underestimates the data at center of mass energies, s $\sim$ 11 GeV.

I. INTRODUCTION

In hadron physics, photoproduction of single pion is essential to understand the photon-nucleon vertex. At low energies, the photon-nucleon coupling establishes excited nucleon resonances which has been at the forefront of physics "missing resonances" search. At high energies single pion photoproduction can be used to test predictions of Regge theory, in which recent calculations [1] have shown to describe the presented data well. Furthermore, these measurements have shown that the differential cross section for single pion photoproduction at fixed c.m. angles, $\theta_{c.m.}$, of 70°, 90° and 110° seem to scale as $\frac{d\sigma}{dt} \sim s^{2-n} f(\theta_{c.m.})$, where s and t are the Mandelstam variables and n is the total number of interacting elementary fields in the initial and final state of the reaction. This is predicted by the constituent counting rule [2, 3] and exclusive measurements in pp and $\bar{p}p$ elastic scattering [4, 5], meson-baryon Mp reactions [5], and photoproduction γN [6–13] agree well with this rule. The following paper details the CLAS g12 experiment, the extraction of single neutral pion photoproduction from data, the differential cross-sections through the entire beam energy range of the g12 experiment, a comparison of the differential cross-section with existing world data, as well as the comparison of the data to the model given in [1] and a comparison to the constituent counting rule.

* Now at Forschungszentrum Jülich; m.kunkel@fz-juelich.de

II. EXPERIMENTAL SETUP

The measurements used for this analysis was taken with the CLAS detector at Hall B at the Thomas Jefferson National Accelerator Facility TJNAF located in Newport News, Virginia. The *g12* experiment is a photoproduction experiment, it ran during March - June 2008 with a total of 44 days of good beam time. It collected over 128 TB of raw data that consisted of $26 \cdot 10^9$ events, with an integrated luminosity of 68 pb^{-1}. The photon beam was produced by impinging a 5.715 GeV electron beam, at 65nA, on a Au radiator of 10^{-4} radiation length. Photons in the energy range from 20% to 95% of the electron beam energy were tagged, resulting in a photon beam energy range of 1.1-5.5 GeV. This photon beam was then collimated before being introduced onto a ℓH_2 target 40 cm in length along the z-direction and 2 cm radius. The placement of the target was 90 cm upstream from CLAS center (toward Au radiator), this increased the acceptance of particles in the forward direction. During the runtime of *g12*, the Cherenkov detectors were filled with perfluorobutane (C_4F_{10}) allowing for electron/positron detection. The experiment had a dedicated trigger, amongst 9 other triggers, that consisted of CC and EC coincidence hits for the entire beam energy range. With proper cuts on the CC and EC a π/e rejection of 10^6 for $e^{\pm}$ pairs was established.

A. *g12* Run Summary

The *g12* experiment was divided into 626 production runs, 37 single-prong runs, 13 special calibration runs and numerous diagnostic runs which were not recorded.

Each run consisted of approximately 50 million triggered events. If a run did not have at least 1M triggered events or if the run was corrupt, the run was discarded. The *g12* experiment had several special calibration runs. These runs consist of normalization, zero-field, and empty-target data runs. The normalization runs were used to calibrate the tagger for the measurement of the total photon flux and consistency of the left and right TDC signals of the tagger. The zero-field data was taken with the main torus magnet off. This was done to account for the position and orientation of the drift-chambers in the reconstruction. The empty target runs were used to investigate the contributions of the target wall to the data sample.

III. EVENT SELECTION

Pions were skimmed initially and then re-identified as leptons by changing the mass of the pion. This method is sufficient when the decaying particle's mass, i.e. m_{π^0}, is less than that of pions. If the event satisfied the requirements listed in Table I, then all TOF, ST, momentum and vertex information was outputted as well as CC and EC information for the $\pi^{\pm}$ particles to be used to identify leptons, as discussed in Sec IV. To reduce the size of the data set, a cut was placed on the total missing mass of $\gamma p \to p\pi^+\pi^-$ to be less than 275 MeV. This cut was broad enough to not interfere with π^0 selection from single π^0 production i.e. $\gamma p \to p\pi^0$ when assigned the pion the lighter mass of a electron/positron. This broad cut also does not interfere with π^0 production from light meson decay, i.e $\gamma p \to p\omega \to p\pi^+\pi^-\pi^0$.

TABLE I. Requirements of initial skim

Requirement
One in-time beam photon
One proton
One π^+ or *"unknown"* of q^+
One π^- or *"unknown"* of q^-

IV. PARTICLE IDENTIFICATION

Lepton identification was based on conservation of mass. Once the data is skimmed according to Table I, all particles that were π^+, π^-, unknown with q^+ or unknown with q^- were tentatively assigned to be electrons or positrons based on their charge. This meant that the mass term of the particle's 4-vector was set to be the mass of an electron instead of that of a pion. This technique works because the mass of the π^0 (0.135 GeV) is less than the mass of π^+ or π^- (0.139 GeV) and by laws of conservation of energy-momentum, a lighter particle cannot decay into heavier particle's.

A. Kinematic Cuts

First it should be noted that for the /g12 experiment, there was a two-prong trigger for events in which the photon beam energy was greater then 3.6 GeV, while for the entire data taking process there was a "lepton" trigger configuration. Therefore to measure the differential cross-section at photon beam energies less than 3.6 GeV this "lepton" trigger information was employed. Once particle section was achieved, it was necessary to reduce the background of the exclusive $\gamma p \to p\pi^+\pi^-$ reaction. For events of photon beam energy less than 3.6 GeV, a CC and EC "hit" must have been recorded for each charge track that was not the proton. For all events 3 kinematic fits were performed, a 1-C ($\gamma p \to pe^+e^-(\gamma)$) to identify the missing photon in the reaction, a 4-C ($\gamma p \to p\pi^+\pi^-$) as a discriminator and a 2-C ($\gamma p \to p\pi^0 \to pe^+e^-(\gamma)$) to identify the reaction. After the kinematic fit, a 1% confidence level cut was placed on the 1-C fit. The missing energy of the $\gamma p \to pe^+e^-$ spectrum versus the missing mass of $\gamma p \to pX$ was analyzed and shown that a 75 MeV cut on the missing energy was suitable to suppress the $\gamma p \to p\pi^+\pi^-$ reaction, see figure 1. After the missing energy cut, the signal to background ratio was $\sim 99.7\%$, see right figure 1, the other 4-C and 2-C fits were then used with a 1% confidence on each to suppress the background to $\sim 99.9\%$.

V. MONTE-CARLO

There are certain kinematic regions of CLAS in which physics events are not being recorded properly i.e. the area dividing each sector in CLAS. Furthermore each sector in CLAS is asymmetric in the acceptance of events due to subsystem inefficiencies such as inoperable DC wires, PMT inefficiencies, dead scintillator strips the the TOF and ST subsystems. When a triggered event is recorded and reconstructed these asymmetric inefficiencies factors are reflected and must be carefully understood because these factors are properties of the CLAS detector and independent of any physics that occurred. To properly understand the detector effects on the data, CLAS utilizes a GEANT simulation package know as GSIM. To prepare an event for GSIM the program GAMP2PART converts a text file, containing the 4-momentum of the generated event, into a suitable file format for GSIM. GSIM then simulates the passage of these particles through the CLAS detector and generates the associated ADC and TDC information from detector hits. GSIM takes into account detector inefficiencies described in the CLAS_CALDB_RUNINDEX. The CLAS_CALDB_RUNINDEX is an array of information about each subsystem's inefficiency that was derived during the *g12* calibration process. The GSIM simulated hits are

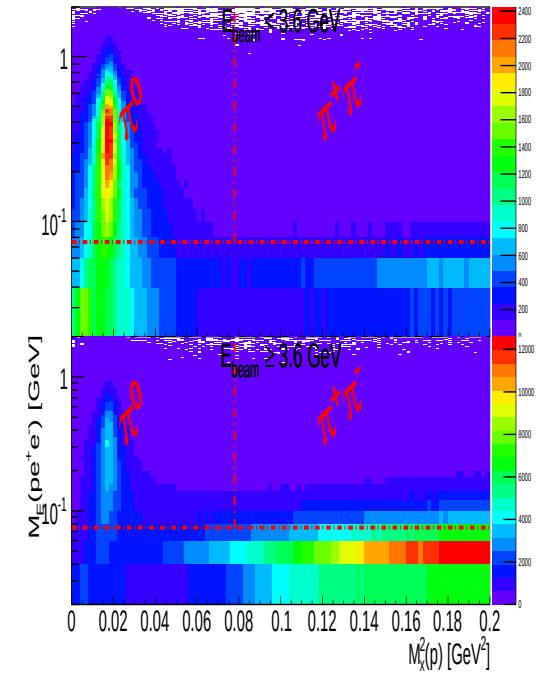

(a)

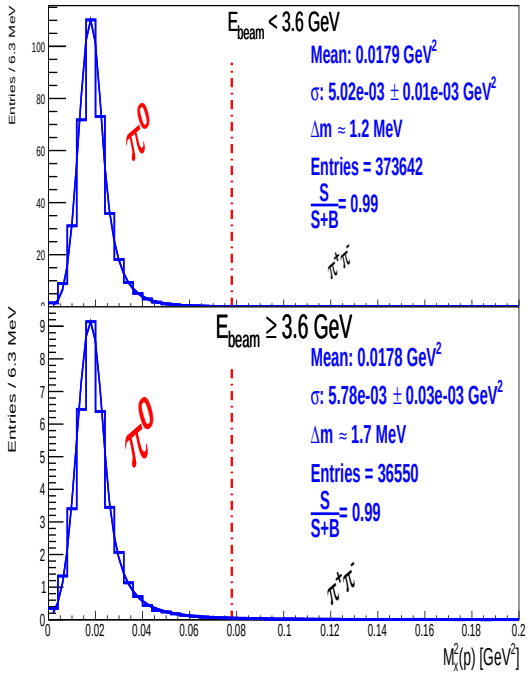

(b)

FIG. 1. Left: $M_x^2(p)$ vs. $M_E(pe^+e^-)$. The horizontal red dashed-dotted line depicts the 75 MeV cut used in this analysis. The vertical red dashed-dotted line depicts the boundary of single π^0 to $\pi^+\pi^-$ production. Right: Final $M_x^2(p)$ data used in analysis. The horizontal red dashed-dotted line depicts the threshold of $\pi^+\pi^-$ production.

then "post-processed" by smearing the TDC and ADC hits to imitate the observed resolution of the detector subsystems using the program GPP (GSIM post-processor). GPP also removes detector hits due to inefficient DC wires.

The acceptance for the cross-sections presented in this work was measured using phase-space Monte-Carlo (MC) simulation, using PLUTO++ [**?**] as the generator, for the reaction channels,

$$\begin{aligned}\gamma \mathrm{p} \rightarrow\ & p\pi^0 \\ & \hookrightarrow p\gamma\gamma \\ & \hookrightarrow pe^+e^-\gamma \end{aligned} \tag{1a}$$

$$\begin{aligned}\gamma \mathrm{p} \rightarrow\ & p\pi^0 \\ & \hookrightarrow pe^+e^-\gamma. \end{aligned} \tag{1b}$$

A total of events, N_g, was generated and this number was weighted by the relative branching ratios found in Table **??** to resemble the conditions of the data. The number of events generated for the reaction channel 1a can be found in Table II as N_c. The number of events generated for the reaction channel n 1b can be found in Table II as N_d. After the events are generated, they are inputted into the CLAS simulation chain GAMP2BOS, GSIM, GPP, and then reconstructed with the same program used to reconstruct the data, a1c, all programs in the simulation chain use the parameters and the run index described above. Once the events are processed through a1c, the cuts described in Secs. **??**, **??**, are applied as they are to the real data. The acceptance $\eta(E_\gamma, \theta^{\pi^0}_{C.M.})$ is then determined by adding the simulations for the conversion and the dalitz, then for photon energy bins of 25 MeV increments and $\Delta\cos\theta^{\pi^0}_{C.M.} = 0.0125$ increments, the ratio of reconstructed events (N_R) to generated events (N_G) yields,

TABLE II. Number of generated events in each decay spectrum

Quantity	Value·10^7	Description
N_g	240	Total number of π^0 events generated
N_c	237	Total number of $\pi^0 \rightarrow \gamma\gamma$ events generated
N_d	2.8	Total number of $\pi^0 \rightarrow e^+e^-\gamma$ generated

$$\eta(E_\gamma, \cos\theta^{\pi^0}_{C.M.}) = \frac{N_R(E_\gamma, \cos\theta^{\pi^0}_{C.M.})}{N_G(E_\gamma, \cos\theta^{\pi^0}_{C.M.})}\ . \tag{2}$$

The $\Delta\cos\theta^{\pi^0}_{C.M.}$ binning in the acceptance is a factor of 2.4 finer than the smallest $\Delta\cos\theta^{\pi^0}_{C.M.}$ increment used in the cross-section measurement. If an accurate physics model for the generator had been used, as was in Sec. V, the binning for the acceptance would not have had to be so fine.

A. Simulating the Lepton Trigger

During the collection process, for an event to be written by the DAQ it must have passed at least one of the trigger "bits" defined in Sec. **??**. As discussed in Sec. **??**, the process of lepton triggering required a coincidence between the EC and the CC subsystems. This coincidence was established by using the voltage sum of the CC for a sector and the voltage sum of the EC for the same sector and comparing each sum to a preset threshold described in Table **??**. However when GSIM simulates tracks through the CC and EC, it does not account for the minimum voltage threshold that was required for data collection, moreover the simulation of the trigger must match the trigger efficiency discussed in Sec. **??**.

Simulation of the CC and EC trigger "bit 6", Sec. **??**, was performed by writing an algorithm that attempted to mimic the method in which triggered data was recorded. To accomplish this a modified function, written by Simeon McAleer from FSU, was written into the simulation reconstruction algorithm. The routine returned the sector and a boolean of 0 or 1 (pass or fail), that simulated the trigger based on the following criteria;

1. The sector with the highest EC summed energy over threshold.
2. The sector with the highest EC Inner Layer summed energy over threshold.
3. The sector with the highest CC summed energy over threshold.
4. All three above conditions must be in same sector.

Thresholds as described in Table **??** are 80 mV, 60 mV and 20 mV for EC *inner*, EC*total* and CC respectively. The CC trigger threshold was applied to groups of eight CC PMTs, called "sim bits". The "sim bits" were staggered by four PMTs so that each PMT goes into two "sim bits", after which all "sim bits" were "*OR*"'d together. If any "sim bit" calculated as above threshold, that specific sector was then compared to the remaining sectors to establish the condition listed in 3.

The EC *inner* and EC *total* trigger thresholds were applied to all EC strips in a sector. This was done by summing over the energy for every strip in every orientation of the EC per sector. If the energy summation for the EC *inner* was above threshold, that specific sector was then compared to the remaining sectors to establish the condition listed in 2. If the energy summation for the EC *total* was above threshold, that specific sector was then compared to the remaining sectors to establish the condition of the sector with the highest EC summed energy over threshold.

1. *Validity of Trigger Simulation*

The actual triggered data could have been triggered by the following sceneries;

1. e^- CC and EC hit above preset thresholds,
2. e^+ CC and EC hit above preset thresholds,
3. e^- CC hit above preset thresholds and e^+ EC hit above preset thresholds in the same sector,
4. e^- EC hit above preset thresholds and e^+ CC hit above preset thresholds in the same sector.

The lepton trigger "bit 6" was 100% efficient (see Sec. **??**) when the data was cut using all the conditions listed above (1, 2, 3, 4) using an "OR" flag. This means that a $\gamma p \rightarrow pe^+e^-$ event must satisfy at least one of the listed conditions. The reduction in events when at least one of the conditions was satisfied was 69.91%. Prior to simulating the trigger, cutting the MC with the listed conditions reduced the event yield by 81.91%. Simulating the trigger and cutting on the MC events with the listed conditions reduced that event yield to 69.48%. This indicates that the trigger simulation is properly mimicking the trigger configuration used when data is collected.

VI. PLUTO++ EVENT GENERATOR

Pluto [**?**] is a Monte-Carlo event generator designed for the study of hadronic interactions and heavy ion reactions in HADES, FAIR and upcoming PANDA collaborations. The versatility of Pluto enables its use as an event generator for photoproduction in CLAS. For hadronic interactions, Pluto can generate interactions from pion production threshold to intermediate energies of a few GeV per nucleon. The entire software package is based on ROOT and uses ROOT's embedded C++ interpreter to control the generation of events. Programming event reaction can be set up with a few lines of ROOT macro code without detailed knowledge of programming. Some features in Pluto are, but not limited to;

- Ability to generate events in phase space.
- Ability to generate events with a continuous bremsstrahlung photon beam.
- Ability to generate events weighted by a user defined t-slope.
- Ability to generate events weighted by a user defined cross-section.
  - Total cross section can be inputted via functional form or histogram.
  - Differential cross sections can be inputted via functional forms or histograms for specific beam energies up to 110 histograms relating to intervals of beam energy.
- Ability to generate events that decay via already established physics parameters, i.e. transition form factors.

- Ability to generate events that decay via modified established physics parameters.
- Ability to generate events with multiple production channels, weighted by user inputted cross-section probability.
- Ability to generate events with multiple decay channels, weighted by user inputted branching ratio.
- Ability to perform vertex smearing.
- Ability to create virtual detectors.

For the analysis presented in this work, Pluto was used in conjunction with known differential cross sections to verify simulation momentum smearing and tagger resolution, Sec. **??**. Pluto was also utilized as a phase space generator in this analysis, to perform a "tune" on the kinematic fitter, Sec. **??**, to calculate the acceptance corrections Sec. **??**, and to calculate the normalization Sec. **??**.

VII. SYSTEMATIC UNCERTAINTIES

Systematic errors are caused the controls of the experiment, such as flux, simulation, density and length of the ℓH_2 target and also systematic errors are caused by various analytical tools used, such as the kinematic fitter.

A. Branching Ratio Systematic Uncertainty

The branching ratios for the two topologies used to measure the cross-section were obtained from PDG [**?**] and are listed again in Table III with their associated errors. Uncorrelated quantities that are summed as,

$$f = \sum_{i=1}^{M} a_i P_i \tag{3}$$

have errors as

$$\sigma_f = \sqrt{\sum_{i=1}^{M} (a_i \sigma_i)^2}. \tag{4}$$

Therefore

$$\frac{\Gamma}{\Gamma_{tot}} = \frac{\Gamma_{\pi^0 \to e^+e^-\gamma}}{\Gamma_{tot}} + \frac{\Gamma_{\pi^0 \to \gamma\gamma \to e^+e^-\gamma}}{\Gamma_{tot}} \tag{5}$$

$$= \frac{\Gamma_{\pi^0 \to e^+e^-\gamma}}{\Gamma_{tot}} + \frac{\Gamma_{\pi^0 \to \gamma\gamma} P(\gamma \to e^+e^-)}{\Gamma_{tot}} \ , \tag{6}$$

where $P(\gamma \to e^+e^-)$ is the probability of photon conversion into e^+e^-. To measure $P(\gamma \to e^+e^-)$, the acceptance for conversion $(P(\gamma \to e^+e^-) \cdot \eta_{e^+e^-})$ is divided by the acceptance for Dalitz $(\eta_{e^+e^-})$. Fig. 2 shows that

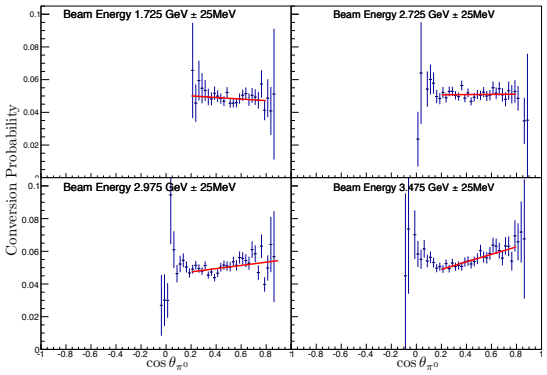

(a)

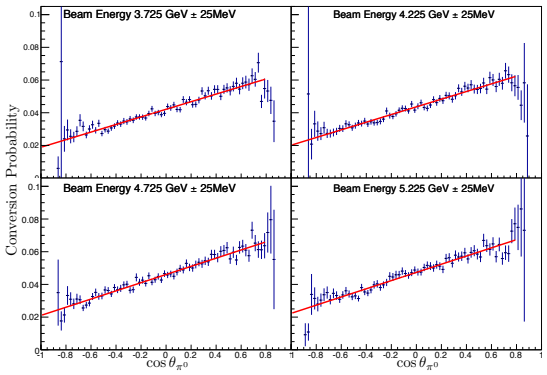

(b)

FIG. 2. Probability of Photon Conversion vs. $\cos\theta$ for various values of E_γ. The maximum probability for this analysis was measured in the top left plot of b.

the conversion probability depends on incident photon energy. A maximum probability of 8% per-photon was measured, shown in Fig 2b top left plot. Therefore

$$\frac{\Gamma}{\Gamma_{tot}} = \frac{\Gamma_{\pi^0 \to e^+e^-\gamma}}{\Gamma_{tot}} + \frac{\Gamma_{\pi^0 \to \gamma\gamma} P(\gamma \to e^+e^-)}{\Gamma_{tot}} = 0.09 \ , \tag{7}$$

and has error

$$\sigma_f = \sqrt{\left(\frac{1}{\Gamma_{tot}}\right)^2 (\sigma^2_{\pi^0 \to e^+e^-\gamma} + \sigma^2_{\pi^0 \to \gamma\gamma})} = 0.0037. \tag{8}$$

The energy and $\cos\theta$ dependence of the conversion is accounted for in the acceptance, which is E_γ and $\cos\theta$ bin-dependent.

TABLE III. Branching ratio and errors used in $\frac{d\sigma}{d\cos\theta^{\pi^0}_{C.M.}d\phi}$ measurements

Quantity	Value	Error
$\Gamma_{\pi^0\to\gamma\gamma}$	0.98823	0.00034
$\Gamma_{\pi^0\to e^+e^-\gamma}$	0.01174	0.00035
$\frac{\Gamma}{\Gamma_{tot}}$	0.13	0.0037

B. Cut Based Systematic Uncertainty

The procedure to determine the systematic uncertainty of the cuts placed on the various kinematic fits was first to calculate an acceptance with a different cut, then to calculate a new total cross-section measurement applying the different cut to the data. The total cross-section was computed at various photon beam energies. Lets denote the original measured total cross-section as Ξ_1 and the new total cross-section determined by the new cut as Ξ_n, then the systematic error was calculated as.

$$\sigma_{cut} = \frac{|\Xi_1 - \Xi_n|}{\Xi_1} \tag{9}$$

Some systematic uncertainty depended on the photon energy. All cut based systematics were performed individually, meaning when a cut was changed, the remaining cuts retained their original value, see Table IV for the values of the cuts that were changed to calculate the systematic error.

TABLE IV. Different Cuts to analyze systematics

Cut	Original	Adjusted	Uncertainty
2-C Fit Pull Probability	1%	10%	0.0219
1-C Fit Pull Probability	1%	10%	$0.00216 + 0.01083E_\gamma$
4-C Fit Pull Probability	1%	10%	0.00031
Missing Energy Cut	75 MeV	100 MeV	0.02781

C. Photon Flux Systematic Uncertainty

The photon flux calculation should be consistent throughout the experiment. If the flux measurement is not consistent due to corrections made with the live-time, beam corrections or fractional difference in the reported current to the actual current during the photon flux normalization run then a systematic uncertainty would be produced. To study this effect we divided the g12 run period into four groups. Table V lists the run groups used for this study. The procedure to determine the systematic error, σ, of the flux is to calculate the accepted and flux corrected yield, Υ^c, for each run group and compare Υ^c to the average accepted and flux corrected yield of all 4 run groups, μ^c. After σ is calculated, it was normalized to $N\mu^c$ as to represent the error as a percentage, which later is added in quadrature and multiplied by the measured cross section to determine the appropriate error.

TABLE V. List of run groups used to determine photon flux systematic error.

Run Group	Range	Total Runs
1	56605-56798	116
2	56799-56980	116
3	56992-57173	116
4	57174-57317	115

$$\sigma_{group} = \sqrt{\sum_{i=1}^{N=4}(\Upsilon_i^c - \mu^c)}, \tag{10}$$

where

$$\mu^c = \frac{1}{N}\sum_{i=1}^{N=4}\Upsilon_i^c \tag{11}$$

$$\sigma_{group}^{normalized} = \frac{\sigma_{group}}{N\mu^c} \tag{12}$$

D. Detector Efficiency Systematic Uncertainty

Each sector in CLAS can be treated as an individual detector, with its own efficiency and resolution. A systematic uncertainty could arise if one or more of the sectors is not simulated properly. The procedure to determine the systematic error, σ, of the sector is to calculate the accepted corrected yield, Υ^c, for each sector and compare Υ^c to the average accepted corrected yield of all 6 sectors, μ^c. After σ is calculated, it was normalized to $N\mu^c$ as to represent the error as a percentage, which later is multiplied by the measured cross section to determine the appropriate error.

$$\sigma_{sector} = \sqrt{\sum_{i=1}^{N=6}(\Upsilon_i^c - \mu^c)}, \tag{13}$$

where

$$\mu^c = \frac{1}{N}\sum_{i=1}^{N=6}\Upsilon_i^c \tag{14}$$

$$\sigma_{sector}^{normalized} = \frac{\sigma_{sector}}{N\mu^c} \tag{15}$$

This calculation was performed for various bins of incoming beam energy to determine the beam energy dependence.

E. z-vertex Cut Systematic Uncertainty

The systematic uncertainty of the z-vertex cut was analyzed by varying the initial vertex cut from $-110 \leq z \leq -70$ to $-109 \leq z \leq -71$ for both data and MC. Afterward the procedure for determining the systematic was identical to the method used to determine the "Cut Based Systematic Uncertainty". The systematic uncertainty from varying the z was 0.0041, shown in Fig. 3

F. Target Systematic Uncertainty

Since the systematic on the density is 0.02%,see Sec **??**, the maximum systematic on the target is due to uncertainty in the length on the target which is 40 cm $\pm$ 0.2 cm. A total systematic on the target was assign to be 0.5%.

G. Total Systematic Uncertainty

The total systematic uncertainty along with a list of the individual systematics is presented in this subsection. The calculation of the total systematic error is

$$\sigma_{tot}^{sys} = \sqrt{\sum_{i=1}^{M} \sigma_i^2} \tag{16}$$

Figure 3 is a pictorial version of Table VI.

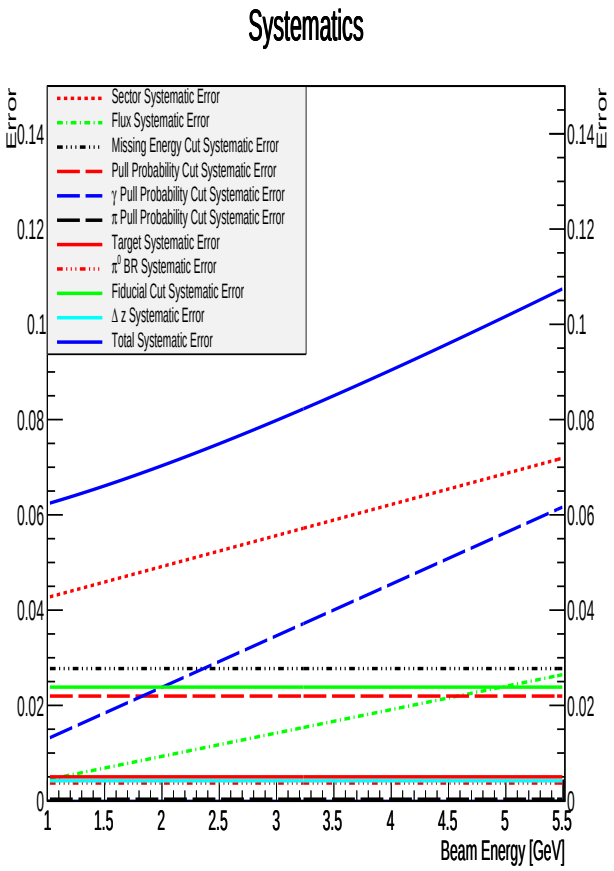

FIG. 3. The contribution of all systematic uncertainties.

TABLE VI. Systematic errors used in $\frac{d\sigma}{d\cos\theta^{\pi^0}_{C.M.}d\phi}$ measurements

Systematic	Error
Sector	$0.0361 + 0.0065E_\gamma$
Flux	$-0.00051 + 0.00491E_\gamma$
Missing Energy Cut	0.02781
2-C Fit Pull Probability	0.0219
1-C Fit Pull Probability	$0.00216 + 0.01083E_\gamma$
4-C Fit Pull Probability	0.00031
Target	0.005
Branching Ratio	0.0037
Fiducial Cut	0.024
z-vertex Cut	0.0041
Total	$\sqrt{(3.2 + 0.51E_\gamma + 0.184E_\gamma^2)} \cdot 10^{-3}$

VIII. COMPARISON WITH THEORETICAL MODELS

There are several models that attempt to describe π^0 photoproduction in the low beam energy resonance region, while in the high beam energy regime there exists limited amount of theory. Described below are two theories.

1. *HandBag Model*

The production of the π^0 meson in photon-proton reactions, for incoming photon beam energies greater than 2.8 GeV, can considered to be a hard exclusive reaction. One approach to study the π^0 photoproduction, is use the handbag model. In the handbag approach, the reaction is factorized into two parts. The first part is when one quark from the incoming and one from the outgoing nucleon participate in the hard sub-process. This hard sub-process is achieved when the incident photon excites a quark, since quarks are bound quantum particles, the excited quark produces a jet of quarks that form the meson and then de-excites back into the nucleon. This is calculable using pQCD. The second part ,the soft part, consists of all the other quarks that are spectators and can be described in terms of GPDs [14–17]. The handbag mechanism is applicable when the Mandelstam variables, s, t, u, are large as compared to a hadronic scale of order 1 GeV . In Ref. [18] a model, derived from the handbag ap-

proach, has been applied to predict angular dependence of scaled photoproduction cross section of π^0 and is illustrated in Fig. 4. The handbag model calculations by Kroll *et al.* [18] does not agree with the measurement obtained by *g12*.

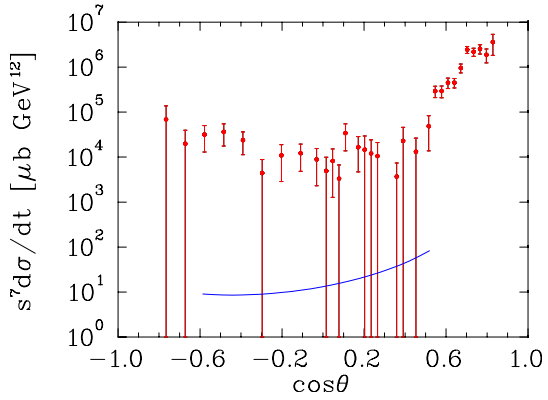

FIG. 4. Comparison of the π^0 differential cross section photoproduction data to GDP handbag model. Experimental data at $s = 11.08$ GeV^2 are from the current (red filled circles). The theoretical prediction at $s = 10$ GeV^2 by [18] is given by blue solid line.

[1] V. Mathieu *et al.*, Phys. Rev. **D92**, p. 074013 (2015), arXiv:1505.02321 [hep-ph].
[2] S. J. Brodsky and G. R. Farrar, Phys. Rev. Lett. **31**, 1153–1156 (1973).
[3] G. P. Lepage and S. J. Brodsky, Phys. Rev. D **22**, 2157–2198 (1980).
[4] P. Landshoff and J. Polkinghorne, Physics Letters B **44**, 293 – 295 (1973).
[5] R. L. Anderson *et al.*, Phys. Rev. D **49** (1994).
[6] W. Chen *et al.* (The CLAS Collaboration), Phys. Rev. Lett. **103**, p. 012301 (2009).
[7] L. Y. Zhu *et al.* (Jefferson Lab Hall A Collaboration), Phys. Rev. Lett. **91**, p. 022003 (2003).
[8] R. A. Schumacher and M. M. Sargsian, Phys. Rev. C **83** (2011).
[9] R. L. Anderson *et al.*, Phys. Rev. D **14**, 679–697 (1976).
[10] J. Napolitano *et al.*, Phys. Rev. Lett. **61**, 2530–2533 (1988).
[11] J. E. Belz *et al.*, Phys. Rev. Lett. **74**, 646–649 (1995).
[12] C. Bochna *et al.*, Phys. Rev. Lett. **81**, 4576–4579 (1998).
[13] E. C. Schulte and others., Phys. Rev. Lett. **87** (2001).
[14] X.-D. Ji, Phys.Rev.Lett. **78**, 610–613 (1997).
[15] X. Ji, Phys. Rev. D **55**, 7114–7125 (1997).
[16] A. Radyushkin, Phys.Lett. **B380**, 417–425 (1996).
[17] M. Diehl, T. Feldmann, R. Jakob, and P. Kroll, Eur.Phys.J. **C8**, 409–434 (1999).
[18] H. W. Huang and P. Kroll, Eur.Phys.J. **C17**, 423–435 (2000).
[19] M. Dugger *et al.*, Phys.Rev. **C76**, p. 025211 (2007), 0705.0816.
[20] M. Dugger *et al.* (CLAS Collaboration), Phys.Rev. **C88**, p. 065203 (2013), 1308.4028.
[21] O. Bartholomy *et al.* (CB-ELSA Collaboration), Phys.Rev.Lett. **94**, p. 012003 (2005), hep-ex/0407022.
[22] V. Crede *et al.* (CBELSA/TAPS Collaboration), Phys.Rev. **C84**, p. 055203 (2011), 1107.2151.
[23] A. Anisovich *et al.*, Eur.Phys.J. **A44**, 203–220 (2010), 0911.5277.
[24] M. Sumihama *et al.*, Phys.Lett. **B657**, 32–37 (2007), 0708.1600.
[25] O. Bartalini *et al.* (GRAAL Collaboration), Eur.Phys.J. **A26**, 399–419 (2005).
[26] M. Braunschweig *et al.*, Physics Letters B **26**, 405 – 409 (1968).
[27] W. Briscoe *et al.*, Institute of Nuclear Studies of The George Washington University Database,.
[28] P. Joss, Compilation of photoproduction data above 1.2 gev, 1970.
[29] M. Fuchs *et al.*, Physics Letters B **368**, 20 – 25 (1996).
[30] R. Beck, Eur. Phys. J. A, **28**, 173–183 (2006).